A

DISTANCE MEASURES

For the sake of simplicity, only the distance between discrete 3D-surfaces represented by triangular meshes will be defined. A discrete 3D-surface is usually represented by a set of point $S = \{p^1, p^2, .., p^n\}$; thus, the similarity between two surfaces is measured by computing distances between the respective points sets.

First, the definition of the point to point Euclidean distance is given, followed by different surface to surfaces distances derived form the Euclidean one.

Euclidean distance between two points

The Euclidian distance is defined as the shortest possible path through space between two points, also called the $L^2 - norm$. Let consider two points p and p' defined in a 3-dimensional space, the distance magnitude is defined as

$$D(p, p') = \|p - p'\|_2 = (\sum_{n=0}^{3} |p_i - p'_i|^2)^{\frac{1}{2}} \tag{A.1}$$

Node to surface distance

The distance $D^s(p, S')$ between the point p and the surface S' is defined as

$$D^s(p, S') = min_{q \in S'} \|p - p'\|_2 \tag{A.2}$$

Minimal distance between two surfaces

The minimal distance between two surfaces S and S' is defined as

$$D^S_{min}(S, S') = min_{p \in S}\{D^s(p, S')\} \tag{A.3}$$

Maximal distance between two surfaces

The maximal distance between two surfaces S and S' is defined as

$$D^{S}_{max}(S, S') = max_{p \in S}\{D^{s}(p, S')\} \tag{A.4}$$

Mean distance between two surfaces

The mean distance between two surfaces S and S' is defined as

$$D^{S}_{mean}(S, S') = \frac{1}{|S|} \sum_{p \in S} D^{s}(p, S') \tag{A.5}$$

where $|S|$ is the number of nodes bellowing the surface S.

Hausdorff distance between two surfaces

The Hausdorff distance (Huttenlocher et al., 1993) between two surfaces is defined as

$$H(S, S') = max\{D^{S}_{max}(S, S'), D^{S}_{max}(S', S)\} \tag{A.6}$$

Modified Hausdorff distance between two surfaces

The modified Hausdorff distance between two surfaces is defined as

$$H(S, S') = max\{D^{S}_{mean}(S, S'), D^{S}_{mean}(S', S)\} \tag{A.7}$$

Dubuisson and Jain (1994) have studied 24 measures to asses the similarities between two discrete surface mesh. According to the authors, Hausdorff distance have the best performance for object matching.

B

Mesh Convergence

In finite element modeling, a finer mesh typically results in a more accurate solution. However, as a mesh is made finer, the computation time increases. To get a mesh that satisfactorily balances accuracy and computing resources, a mesh convergence study was performed

In this scope, the breast and muscle geometries was meshed with different mesh sizes; the minimal elements sizes was set to $7mm$ and the maximal element size was varied between $\{7mm, 10mm, 13mm, 15mm, 17mm, 20mm\}$. The compression paddles geometries were meshed with a constant element size of $1mm$. The number of elements obtained for each mesh size is given in Table B.1. For the mesh size equal to 17 mm, a higher number of elements is obtained then compared to the mesh size of 15mm. As mesh size is defined by the maximal and minimal elements size, a higher number of *small* elements was needed to cover the areas smaller than the *large* elements. In such meshes the elements density is normally concentrated on the geometry's corners or narrow spaces which, in our case, dose not coincide with the region of interest.

Mesh size	20mm	17mm	15mm	13mm	10mm	7mm
Nb. of elements	8367	10897	8099	10751	18453	65785

Table B.1: Number of elements obtained for each mesh size.

As the model was conceived to model breast deformations under compression, an equivalent simulation was performed to estimate the optimal mesh size. Starting from the breast supine geometry, the gravity was applied in the posterio-anterior direction. Then, the right breast was compressed between the compression paddles (Figure B.1). The strain distribution over the breast volume as well as the compression force for each mesh size are given in the Figure B.1.

One can see that the force intensity converges from a mesh size equal to $15mm$, however the strain distribution over the breast volume have still a poor estimation when compared to the strain distribution obtained with a mesh size equal to 7mm. The visual analysis of

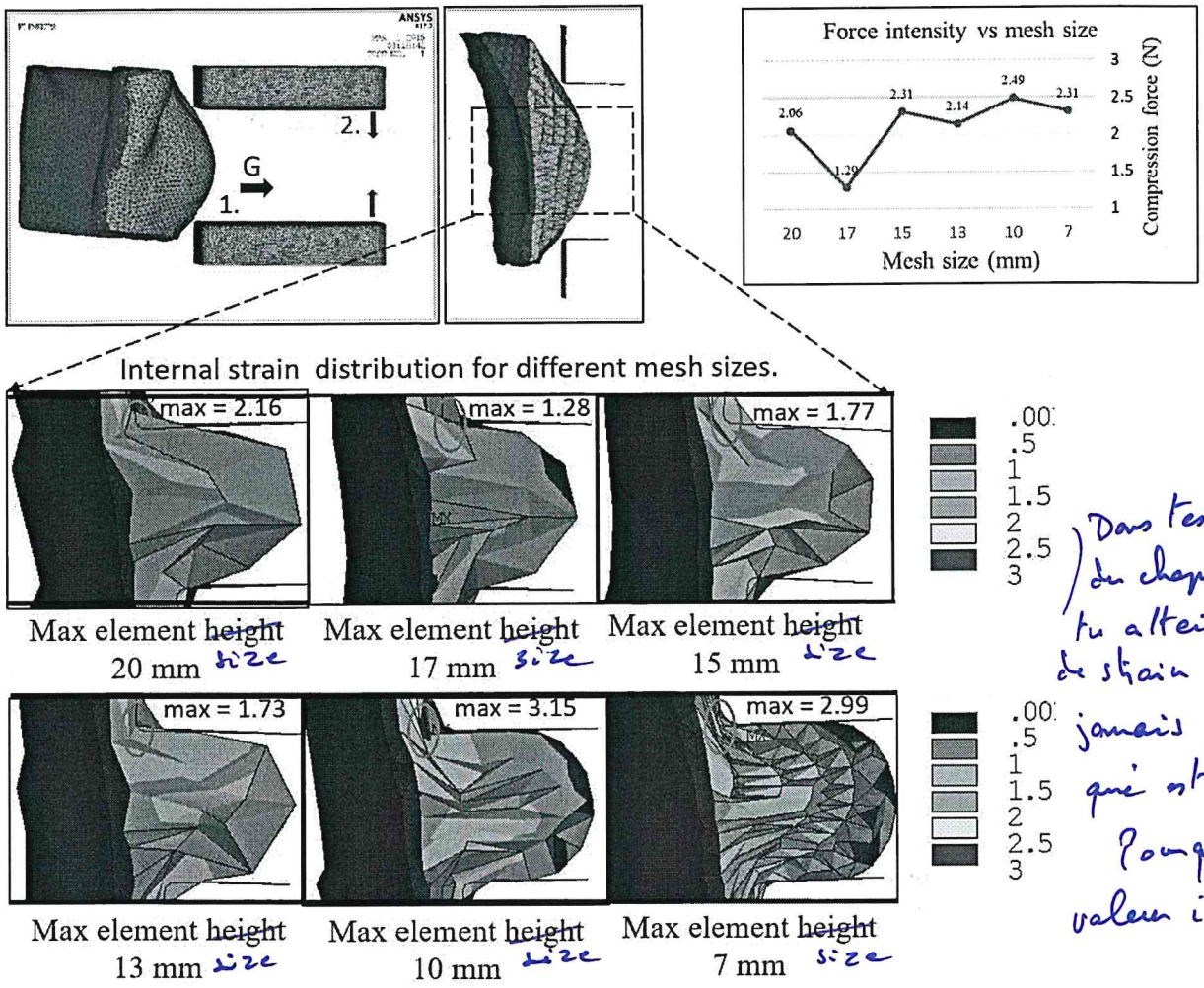

Dans tes simulations du chapitre 5, tu atteins 1.4 de strain mais jamais 3, ce qui est énorme. Pourquoi cette valeur ici ?

Figure B.1: Internal strain distribution in function of the elements size.

the strain distribution and amount of penetration at the surface contact shows that stating from a mesh size equal to 10mm, the results are well enough estimated.

starting ?

C

Bondary conditions
contact models

The proposed biomechanical model consists of two bodies, one representing the pectoral cage and the second represents the breast soft tissues. Between the two bodies, a contact surface is defined in order to model tissues mechanics at the juncture interface.

The next section describes the implementation of different interaction models tested during the model development process. Since the breast tissues are always attached to the pectoral muscle (Figure C.1), the contact surface was modeled using *bonded* and *no-separation frictional* interaction models only.

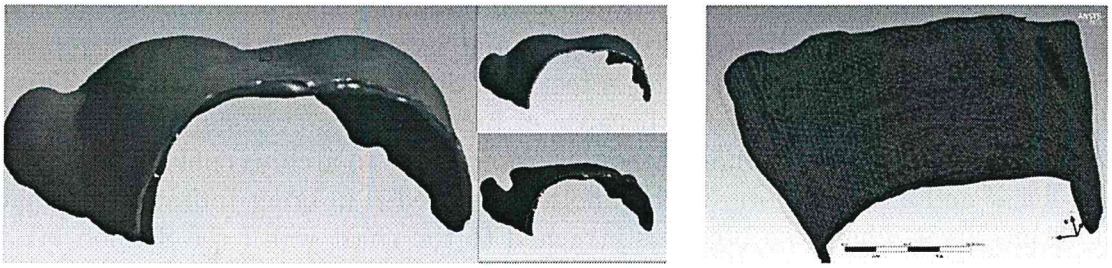

Figure C.1: The two bodies representing the thoracic cage and breast with the associated contact surface. Blue surface- the target surface, red surface - contact surface

The results for pure bonded and pure no-separation sliding models as well as one combined contact surface are listed bellow. For some contacts models, because of ~~important~~ ~~solution~~ instabilities or a poor fidelity to the real breast mechanics only partial results are presented.

Bonded contact surface

First a pure bounded contact was used to model the interaction between the breast and the muscle. To achieve realistic breast deformation, extremely low values of equivalent Young's

modulus and Poisson ratio were needed ($\lambda_{breast} = 0.3kPa$ and $\nu_{breast} = 0.45$). An example of breast deformation in prone and supine configuration is illustrated in Figure C.2.

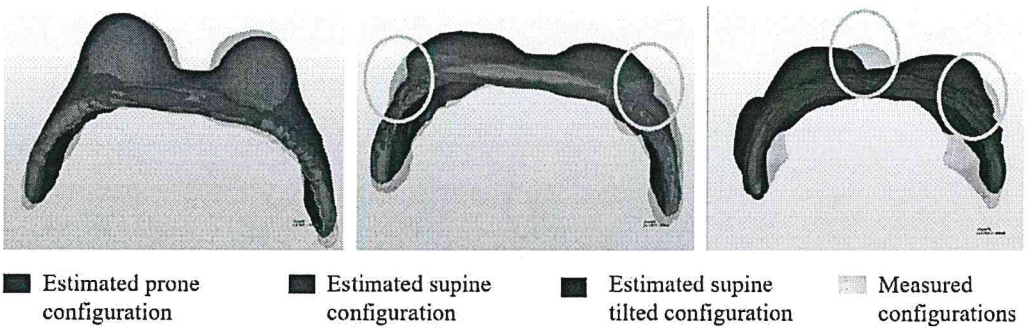

Figure C.2: Resulting breast deformation with a bonded contact model.

One can see that, even if the breast geometry in prone position is well estimated, the ones in supine and supine tilted configurations are constrained laterally. Moreover, a important volume variation was observed which is not a characteristic of breast changes under gravity loading. The volume variation is due to a low value of the Poisson ratio.

Sliding contact surface

Pure sliding contact surface was considered in order to allow more tissues displacement on lateral direction. The breast sliding over the muscle surface was modeled using the Coulomb friction low (Section 2.3.2). Additional boundary condition were set by imposing zero-displacement on the right, left, superior and inferior mesh boundaries representing the breast volume (see Figure 3.10 for a recall on different mesh boundaries). This model caused large convergence problems because of breast tissues over-sliding. It was obvious that the model needs more boundary conditions in order to archive convergence. Moreover a non-linear and a non-uniform sliding model was needed in order imitate the behavior of rich fibrous areas where the breast is attached to the chest wall (see Section 1.1.3 for a recall on breast anatomy).

Mixt contact surface

In order to limit breast tissues sliding a mixt contact surface is defined. Herein, the contact surface consist of two complementary areas (Figure C.3), one modeled as bounded contact and the second one modeled as no-separation sliding contact. The regions corresponding to the bounded contact are defined following the anatomical structures where the concentration of fibrous tissues is significantly high. Such regions are encountered along the muscle surface where the superficial muscle fascia meets the breast suspensory ligaments as the inframammary ligament, deep medial ligament or deep lateral ligament.

Using such a contact model have improved substantially the estimate of the supine breast configuration. However, because of a high deformation gradient imposed at the

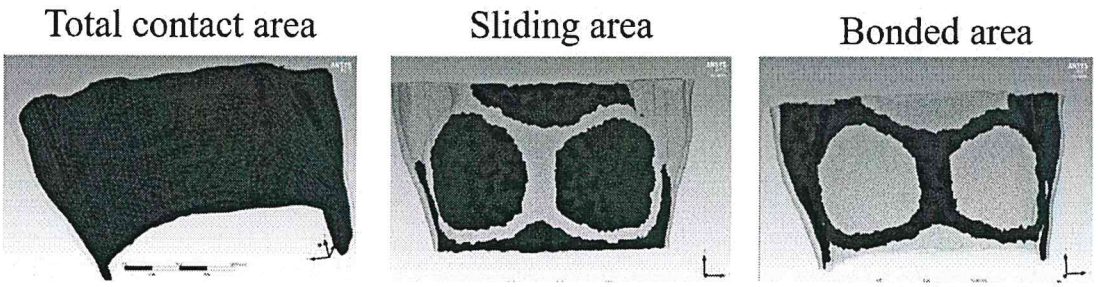

Figure C.3: The contact surface divided in two regions: sliding region and bonded region.

juncture border between the two contact areas, solution convergence problems were meet. Moreover, when the supine configuration is estimated, several fold are created at the skin surface (Figure C.4). Same types of folds were obtained in supine tilted configuration creating large convergence problems because of tissues superposition.

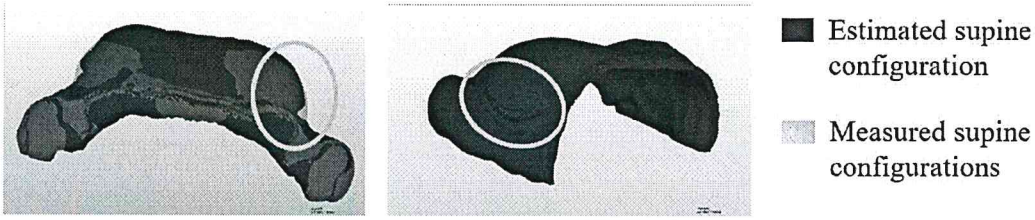

Figure C.4: The contact surface divided in two regions: sliding region and bonded region.

The last described model have provided satisfactory results, however its implies important solution convergence problems. Therefore, the model was improved by replacing the bonded contact regions with stiff ligaments connecting the breast tissues to the muscle. Contrary to the bonded contact, the ligaments preclude progressively the breast tissues from sliding and allows a slight displacement avoiding the folds creation. Moreover, an additional layer modeling the deep layer of breast superficial fascia was added at the juncture surface between breast and muscle. Knowing that the fascia is stiffer than the breast soft tissues, its control the amount of sliding and facilitate the solution convergence. For more information on ligaments and fascia mechanical properties, see the Section 3.4.